SCISPACE
formerly Typeset

Open access • Posted Content • DOI:10.1101/2020.03.01.972216

# Visualizing synaptic plasticity in vivo by large-scale imaging of endogenous AMPA receptors — Source link

Austin R. Graves, Austin R. Graves, Richard H. Roth, Han L. Tan ...+15 more authors

**Institutions:** Discovery Institute, Johns Hopkins University School of Medicine, Johns Hopkins University

**Published on:** 02 Mar 2020 - bioRxiv (Cold Spring Harbor Laboratory)

**Topics:** Synaptic plasticity and AMPA receptor

Related papers:

- Visualizing synaptic plasticity in vivo by large-scale imaging of endogenous AMPA receptors
- Synaptic optical imaging platforms: Examining pharmacological modulation of neurotransmitter release at discrete synapses
- Advanced Fluorescence Protein-Based Synapse-Detectors.
- Editorial: Imaging Synapse Structure and Function.
- Synaptic physiology: illuminating the road ahead.

Share this paper:

View more about this paper here: https://typeset.io/papers/visualizing-synaptic-plasticity-in-vivo-by-large-scale-56qb6y4qt0

bioRxiv preprint doi: https://doi.org/10.1101/2020.03.01.972216; this version posted March 2, 2020. The copyright holder for this preprint (which was not certified by peer review) is the author/funder. All rights reserved. No reuse allowed without permission.

# Visualizing synaptic plasticity in vivo by large-scale imaging of endogenous AMPA receptors

Austin Graves[1,2,*], Richard Roth[1,*], Han Tan[1,*],Qianwen Zhu[1,*], Alexei Bygrave[1,*], Elena Lopez-Ortega[1], Alina Spiegel[1,2], Ingie Hong[1], Richard Johnson[1], Joshua Vogelstein[2,3,4], Daniel Tward[2,3,4], Michael Miller[2,3,4], Richard Huganir[1,2,#]

[1]Department of Neuroscience, Johns Hopkins University School of Medicine
[2]Kavli Neuroscience Discovery Institute
[3]Center for Imaging Science, Johns Hopkins University School of Engineering
[4]Department of Biomedical Engineering, Johns Hopkins University
*Equal contribution
[#]For correspondence: rhuganir@jhmi.edu

bioRxiv preprint doi: https://doi.org/10.1101/2020.03.01.972216; this version posted March 2, 2020. The copyright holder for this preprint (which was not certified by peer review) is the author/funder. All rights reserved. No reuse allowed without permission.



## Summary

Elucidating how synaptic molecules such as AMPA receptors mediate neuronal communication is crucial to understanding cognition and disease, but current technological barriers preclude large-scale exploration of molecular dynamics in vivo. We have developed a suite of innovative methodologies that break through these barriers: a transgenic mouse line with fluorescently tagged endogenous AMPA receptors, two-photon imaging of hundreds of thousands of labeled synapses in behaving mice, and machine-learning-based automatic synapse detection. Using these tools, we can longitudinally track how the strength of individual synapses changes during behavior. We used this approach to generate an unprecedentedly detailed spatiotemporal map of synaptic plasticity underlying sensory experience. More generally, these tools can be used as an optical probe capable of measuring functional synapse strength across entire brain areas during any behavioral paradigm, describing complex system-wide changes with molecular precision.

bioRxiv preprint doi: https://doi.org/10.1101/2020.03.01.972216; this version posted March 2, 2020. The copyright holder for this preprint (which was not certified by peer review) is the author/funder. All rights reserved. No reuse allowed without permission.



## Introduction

Recent applications of genetically encoded calcium indicators and high-density silicon electrodes have revolutionized our understanding of the cellular and circuit basis of behavior; however, technological barriers preclude similar exploration of the molecular basis of these processes in vivo. To investigate the physiological function of complex molecular systems in vivo, we require techniques to visualize endogenous proteins. Modern proteomic and transcriptomic methods provide biologists with myriad candidate proteins, but in many cases, there are no tools available to effectively study these targets at the level of endogenous proteins in vivo. For example, we are far from having reliable antibodies for the entire proteome, and even when antibodies are available, there are concerns regarding their target specificity. Another approach is to fluorescently tag proteins to visualize their dynamic expression in living tissue. Combined with in vivo two-photon microscopy, this approach enables detailed investigation of the molecular mechanisms underlying complex physiological and pathological systems.

AMPA-type glutamate receptors (AMPARs) are a crucial molecule to study in order to understand the function and dynamics of the nervous system. AMPARs mediate the majority of fast excitatory synaptic transmission in the brain and their regulation is regarded as a key mechanism underlying long-lasting changes in synaptic efficacy that give rise to learning and memory (Huganir and Nicoll, 2013; Malinow and Malenka, 2002). Long-term potentiation (LTP) is characterized by increased AMPAR trafficking to the postsynaptic membrane and associated spine enlargement, which together result in a long-lasting increase in synaptic efficacy; whereas long-term depression (LTD) is characterized by removal of postsynaptic AMPARs, resulting in attenuated synaptic transmission (Anggono and Huganir, 2012; Nicoll, 2017). Impaired regulation of synaptic plasticity is associated with human neurological and psychiatric disease (Berryer et al., 2013; Henley and Wilkinson, 2016; Volk et al., 2015). Despite this clear link between synaptic plasticity and learning, as well as a thorough understanding of molecular mechanisms regulating AMPAR trafficking, very little is known regarding how changes in plasticity are distributed among trillions of synapses throughout the brain. In contrast to advanced strategies to observe and manipulate neuronal activity – using genetically encoded calcium indicators (Dombeck et al., 2010; Lin and Schnitzer, 2016; Xu et al., 2012) or optogenetics (Fenno et al., 2011), respectively – there are currently no methods to physiologically measure postsynaptic strength in vivo on a brain-wide scale.

To overcome this barrier, we developed a transgenic knockin mouse line wherein the AMPAR GluA1 subunit is tagged with super ecliptic pHluorin (SEP), a pH sensitive variant of GFP that fluoresces at neutral pH and is quenched at acidic pH (Miesenbock et al., 1998). When coupled to the extracellular N-terminal domain of the AMPAR, this SEP tag reports the concentration of functional receptors at the cell surface, as the fluorescence of receptors localized in acidic compartments such as endosomes and Golgi is quenched. Our genetic labeling strategy also avoids confounds arising from manipulation of the AMPAR c-terminus, a region important for proper function and trafficking to the postsynaptic membrane (Sheng et al., 2018; Zhou et al., 2018). Many groups have used overexpression of SEP-tagged AMPARs in neuronal culture to study AMPAR trafficking in vitro (Araki et al., 2015; Ashby et al., 2004; Kopec et al., 2006;

bioRxiv preprint doi: https://doi.org/10.1101/2020.03.01.972216; this version posted March 2, 2020. The copyright holder for this preprint (which was not certified by peer review) is the author/funder. All rights reserved. No reuse allowed without permission.



Makino and Malinow, 2009; Patterson et al., 2010; Roth et al., 2017). In addition, previous work using overexpression of SEP-tagged AMPARs in vivo has provided valuable insights regarding the molecular mechanisms of behaviorally relevant plasticity (Diering et al., 2017; El-Boustani et al., 2018; Makino and Malinow, 2009; Roth et al., 2019; Zhang et al., 2015), but these methods enable receptor visualization in only a sparse subset of cells and exogenous overexpression can result in protein mistargeting and dysregulation. The novel genetic labeling strategy presented here avoids these confounds, allowing visualization of endogenous AMPAR expression in a manner that does not impair synaptic function, plasticity, or behavior. Used in conjunction with in vivo two-photon microscopy, this novel SEP-GluA1 knockin mouse is the first tool that enables longitudinal tracking of synaptic plasticity underlying behavior at brain-wide scale with single-synapse resolution.

## Results

### SEP-GluA1 knockin mouse line labels excitatory synapses

Using homologous recombination, we generated a mouse knockin line that inserts SEP into the N-terminus of GluA1. Homozygote knockin mice are viable, breed well, and appear to be physiologically and behaviorally normal (see below). This approach fluorescently labels all GluA1-containing AMPARs in the mice (Fig. 1A-C), enabling robust visualization of excitatory synapses throughout the entire brain. We did observe a decrease in GluA1 mRNA and protein expression in our homozygote knockin line compared to wild type (WT; Fig. 1D-F) most likely due to instability of the resulting mRNA. We also observed a slight increase in GluA2 and GluA3 expression. Using biochemical fractionation to isolate synapses, we observed reduced expression of GluA1 in the postsynaptic density (PSD, 57% of WT mice) and in total protein levels (P2, 44% of WT mice) (Fig. 2E-F).

To validate the physiological function of our knockin line, we made whole-cell voltage-clamp recordings from acute slices of WT and homozygous SEP-GluA1 littermates. We observed no deficits in synaptic physiology or receptor trafficking between WT and SEP-GluA1 mice (Fig. 2). Our electrophysiological data in particular support that synapses with fluorescently labeled AMPARs function identically to WT synapses, with no discernable differences in the amplitude, frequency, or kinetics of miniature excitatory postsynaptic currents (mini EPSCs; Fig. 2A-C) or rectification of the EPSCs (Fig. 2D-E). We also observed that SEP-tagged GluA1 receptors were properly trafficked to the postsynaptic site and colocalized normally with other postsynaptic proteins, such as PSD-95 (Fig. 2F-G). There was a highly significant correlation between the SEP signal and immunofluorescence intensity of both PSD-95 and c-terminal GluA1 antibodies, indicating that all GluA1 receptors express SEP in our knockin mouse line (Fig. 2H-I).

### Intact synaptic plasticity and normal behavior in SEP-GluA1 knockin mice

Homeostatic and Hebbian plasticity are the two major forms of synaptic plasticity that function cooperatively to keep neural circuits stable and plastic, respectively (Bliss and Lomo, 1973; O'Brien et al., 1998; Turrigiano et al., 1998). This novel knockin line represents a powerful tool to study both of these mechanisms, as they are each known

bioRxiv preprint doi: https://doi.org/10.1101/2020.03.01.972216; this version posted March 2, 2020. The copyright holder for this preprint (which was not certified by peer review) is the author/funder. All rights reserved. No reuse allowed without permission.



to be expressed via dynamic regulation of AMPARs. To evaluate if homeostatic plasticity is intact in our knockin line, we made primary cultures of cortical neurons from homozygous SEP-GluA1 mice and WT littermates and treated them with either bicuculline or TTX for two days to induce up- or down-scaling, respectively (Fig. 3A-B). As expected, WT neurons exhibited a significant reduction of surface AMPARs following bicuculline treatment and showed an elevation of surface GluA1 and GluA2 after TTX treatment. SEP-GluA1 KI neurons displayed a similar bidirectional change of surface AMPARs during bicuculline and TTX treatments, indicating comparable homeostatic plasticity in SEP-GluA1 and WT mice. To assess Hebbian plasticity, we compared the expression of long-term potentiation (LTP) in WT and homozygous SEP-GluA1 littermates (Fig. 3C-E) as GluA1 knockout mice show deficits in LTP (Zamanillo et al., 1999). Whole-cell voltage-clamp recordings of synaptically evoked EPSCs were performed in 3-4 week-old mice. After a baseline period of at least 5 minutes, a pairing stimulus consisting of 2-Hz synaptic stimulation and somatic depolarization to 0 mV was delivered, after which we resumed monitoring the amplitude of evoked EPSCs (Fig. 3D). This pairing protocol induced a long-lasting increase in EPSC amplitude in both WT and knockin neurons (n=8 cells from each genotype), consistent with the induction of LTP. We observed no differences in either the induction or expression of LTP between WT and SEP-GluA1 littermates (Fig. 3E). Overall, these data strongly support that our transgenic labeling strategy does not impair synaptic transmission and plasticity.

To further validate our SEP-GluA1 knockin line, we conducted a battery of behavioral experiments using homozygous SEP-GluA1 mice (9 females and 7 males) and WT (9 females and 9 males) littermates (aged 6-10 weeks), as GluA1 knockout mice show deficits in several behaviors, including locomotor activity, anxiety, and spatial memory (Bannerman et al., 2004; Boerner et al., 2017; Bygrave et al., 2019; Sanderson et al., 2007). We assessed locomotor activity by placing animals in an open arena and measuring the number of beam breaks during a 30-minute session. We observed no differences in the time course or total number of beam breaks between WT and SEP-GluA1 mice (Fig. 4A-B). Anxiety was assessed using an elevated plus maze, consisting of two closed arms and two open arms, suspended above the ground. We observed no differences in time spent in the open arms between WT and SEP-GluA1 mice (Fig. 4C-D). Spatial short-term memory was assessed using a Y maze, consisting of three arms and surrounded by distal spatial cues. During the initial exposure phase, one arm was blocked with a clear plexiglass barrier. After exploring the two unblocked arms of the maze, mice were returned to their home cage for 1 min, and then re-exposed to the maze for the test phase, wherein the barrier was removed. WT and SEP-GluA1 mice displayed a similar preference for the novel arm (Fig. 4E-F). Overall, these data strongly support that our transgenic labeling strategy does not impair behavior, as SEP-GluA1 mice display comparable locomotion, anxiety, and short-term memory to WT animals.

**SEP-GluA1 reports synaptic plasticity in vitro**

To examine the function of individual SEP-GluA1 labelled synapses, we used whole-cell voltage-clamp recordings from primary cultures of homozygous SEP-GluA1 pyramidal neurons to measure evoked responses with two-photon glutamate uncaging. To visualize dendritic spines, neurons were filled with a red fluorescent dye via the patch pipette. Glutamate uncaging was targeted to the tips of spine heads (Fig. 5A) and

bioRxiv preprint doi: https://doi.org/10.1101/2020.03.01.972216; this version posted March 2, 2020. The copyright holder for this preprint (which was not certified by peer review) is the author/funder. All rights reserved. No reuse allowed without permission.



the resulting uncaging-evoked excitatory postsynaptic current (uEPSC) was recorded (Fig. 5B). We found a highly significant correlation between SEP-GluA1 fluorescence intensity and uEPSC amplitude (Fig. 5C), indicating that SEP fluorescent intensity can be used as a proxy for synaptic strength.

We further used the SEP-GluA1 knockin line to track changes in synaptic strength following induction of synaptic plasticity in vitro in primary cultures of hippocampal neurons. Using two-photon imaging, glutamate uncaging, and whole-cell patch-clamp recordings, we tracked SEP intensity and functional synaptic strength of spines that received high-frequency glutamate uncaging paired with postsynaptic depolarization versus spines that did not receive this pairing. We found that this pairing stimulus significantly increased uEPSC amplitude and SEP fluorescence in stimulated spines ($n=10$ spines; $p<0.01$ relative to baseline, 1-way ANOVA), consistent with induction of LTP; whereas spines that received only postsynaptic depolarization unpaired with glutamate uncaging did not display similar changes ($n=42$ spines; Fig. 5D-F). This highlights the power of the SEP-GluA1 knockin line to monitor synaptic strength and plasticity via fluorescence imaging.

**Developing computational tools to detect and track labeled synapses in vivo**

To observe AMPAR dynamics in living mice, we implanted cranial windows over somatosensory cortex in homozygous SEP-GluA1 mice and used two-photon microscopy to visualize endogenously labeled synapses (Fig. 6). The observed bright, punctate fluorescence reflects synaptic enrichment of GluA1, likely corresponding to the functional complement of GluA1-containing AMPARs at the PSD (Fig. 6B). Given the richness and scale afforded by this knockin line (Fig. 6C, see also Fig. 1C), which endogenously labels all GluA1-containing synapses throughout the brain, manual annotation of labeled synapses was not feasible. Thus, to automatically detect and segment hundreds of thousands of SEP-labeled synapses, we developed an unsupervised machine learning algorithm based on 3D Wiener filtering, employing pre-whitened matched templates based on the mean appearance of conspicuous puncta and background noise. This approach enabled flexibility to tune segmentations based on accuracy criteria, such as tradeoffs between sensitivity and specificity, as well as prior information about synapse size and shape.

To validate this algorithm, we manually annotated thousands of individual SEP-GluA1 synapses from in vivo volumes of somatosensory cortex (Fig. 6B). We defined ground truth as positive agreement (overlap of ROIs) between two expert annotators. Our detection algorithm yields 85% agreement with ground truth, which exceeds the agreement between two expert human annotators (70%). When used in conjunction with a cell fill to visualize dendritic morphology (Fig. 6D), the punctate enrichment of SEP-GluA1 in spine heads was readily apparent, as 66% of spines overlapped with an automatically detected SEP puncta, defined as edge-to-edge separation between spine and SEP puncta <0.25 μm (Fig. 6E). This overlap was substantially higher than chance, as the distance between spines (red channel) and their nearest SEP neighbor (green channel) increased dramatically when the red channel was rotated relative to green (Fig. 6E). SEP-GluA1 synapses were detected at a uniform rate across depth within layer 1 (L1) of barrel cortex, up to 100μm below the pia surface (Fig. 6F).

bioRxiv preprint doi: https://doi.org/10.1101/2020.03.01.972216; this version posted March 2, 2020. The copyright holder for this preprint (which was not certified by peer review) is the author/funder. All rights reserved. No reuse allowed without permission.



**SEP-GluA1 reports synaptic plasticity underlying sensory stimulation**

To demonstrate the utility of the SEP-GluA1 line and our machine learning algorithm, we investigated synaptic dynamics in barrel cortex during whisker stimulation. Mouse somatosensory cortex displays an exquisite somatotopic map, in which each individual whisker is represented by a discrete cortical area. These so-called barrels provide an ideal tableau to investigate activity-dependent plasticity underlying the encoding of sensory stimulation. Previous work has shown that whisker stimulation (10 Hz) can induce a NMDA receptor dependent LTP in layer 2/3 cells (Holtmaat et al., 2009; Zhang et al., 2015). We surgically implanted cranial windows over barrel cortex in adult SEP-GluA1 mice (2-4 months old). Using optical intrinsic imaging during passive whisker stimulation, we identified barrels corresponding to the C2 and D3 whiskers (Fig. 7A). We imaged SEP-GluA1 expression at high resolution within 100µm cubed volumes of somatosensory cortex. By registering volumes to vasculature and other fiducial markers, we were able to longitudinally image the same cortical volumes in each barrel for at least three hours. To confine our analysis to precisely the same neural volumes throughout sensory stimulation, we further employed post-hoc rigid-body transformations to align the neural volumes imaged over time.

We were able to detect hundreds of thousands of synapses in each mouse and extracted their SEP-GluA1 fluorescence intensity at each time point. To investigate synaptic dynamics at baseline and during sensory stimulation, we delivered 10-Hz mechanical stimulation exclusively to the C2 whisker in lightly anesthetized animals. Whereas the unstimulated barrel displayed a stable distribution of SEP-GluA1 intensity over time, the barrel corresponding to the mechanically stimulated whisker displayed a significant rightward shift in the distribution of SEP-GluA1 intensity, consistent with the induction of LTP (Fig. 7B-E). This potentiation manifested as an increase in the mean SEP-GluA1 intensity (Fig. 7D) as well as increased synapse size (Fig. 7E). The number of detected synapses in both the stimulated and unstimulated barrels was stable over time (Fig. 7F), suggesting that the observed plasticity was not expressed via net spinogenesis or pruning, but rather by a net potentiation of existing synapses.

**Discussion**

A central goal of neuroscience is to understand high-order cognitive functions in terms of their constituent components. Over the past 50 years, we have learned a great deal regarding the general role of synaptic plasticity in learning and memory. While seminal experiments have clearly implicated regulation of AMPARs as a central mechanism to modify the strength of synaptic communication between neurons (Andersen et al., 1977; Frey and Morris, 1997; Huganir and Nicoll, 2013; McNaughton et al., 1978), there is currently a dearth of methodologies to investigate how these molecular dynamics are distributed within vast networks of billions of synapses throughout the brain. For instance, patch-clamp recordings provide excellent spatial and temporal resolution, enabling investigation of how integration of specific synaptic inputs is dynamically tuned by plasticity (Spruston, 2008), but the scale of these recordings is limited to single neurons and performing them in behaving animals is challenging (Bittner et al., 2017; Epsztein et al., 2011). In vivo calcium imaging and high-channel-count electrophysiology offer superb spatial coverage, enabling investigation of neuronal activity within circuits of hundreds of neurons during behavior (Juavinett et al.,

bioRxiv preprint doi: https://doi.org/10.1101/2020.03.01.972216; this version posted March 2, 2020. The copyright holder for this preprint (which was not certified by peer review) is the author/funder. All rights reserved. No reuse allowed without permission.



2019; Jun et al., 2017; Sofroniew et al., 2016), but these techniques lack the spatial resolution to study plasticity of individual synapses. In vivo structural imaging has provided valuable insights regarding how spine formation and elimination has been shown to contribute to neuronal development and synaptic plasticity (Bhatt et al., 2009; Holtmaat and Svoboda, 2009; Holtmaat et al., 2006; Trachtenberg et al., 2002; Xu et al., 2009; Yang et al., 2009), though this method does not measure plasticity at existing spines. In addition, spine size has been reported to be proportional to synaptic strength (Matsuzaki et al., 2001), but this is at best an indirect readout of synaptic strength, and in certain conditions spine size and synapse strength are completely dissociated (Lee et al., 2012; Sdrulla and Linden, 2007; Zhang et al., 2015). Thus, our understanding of how the brain represents learning, memory, and behavior is constrained by currently available methodologies.

Here, we present a suite of novel tools and approaches that bridge this gap, enabling visualization of synaptic plasticity with molecular resolution at brain-wide scale in living animals. At the heart of this suite lies the newly generated SEP-GluA1 mouse, a transgenic knockin line that fluorescently labels all endogenous GluA1-containing AMPARs throughout the entire brain. This line enables direct investigation of the molecular dynamics underlying synaptic plasticity at any scale, from super-resolution synaptic imaging in primary cultures to circuit-level analyses of plasticity in acute slices to brain-region-wide imaging of synaptic strength in behaving animals. The sequence linking the SEP tag and AMPAR N-terminus is known to affect protein expression and proper postsynaptic targeting of the receptor, as previous attempts to fluorescently tag AMPARs at the N-terminus have been reported to result in impaired synaptic function (Diaz-Alonso et al., 2017; Nabavi et al., 2014). However, in our experiments, the N-terminal linkers were lengthened and optimized to increase the flexibility of the SEP tag, thereby limiting disruption of GluA1 function. In the present study, we conducted extensive validation of our novel transgenic line, demonstrating that SEP-GluA1 mice exhibit normal synaptic physiology, AMPA receptor trafficking, and general behavior that is indistinguishable from WT littermates, thereby supporting that our endogenous labeling strategy does not impair synaptic function in any detectable manner. Using both primary cultures and acute slices, we showed that the SEP-GluA1 line is an effective tool to study several forms of AMPAR-mediated plasticity, including homeostatic scaling and long-term potentiation. Using two-photon glutamate uncaging, we clearly demonstrated that the intensity of SEP fluorescence directly correlates with functional synaptic strength, indicating that this line can be used as an effective tool to study synaptic plasticity in vivo. Finally, we developed a machine-learning algorithm to automatically detect and segment extremely large numbers of individual labeled synapses across entire brain regions in living animals. Using these tools, we were able to longitudinally track synaptic plasticity encoding sensory stimulation with unprecedented spatial coverage and molecular resolution, producing the most detailed spatiotemporal map of behaviorally relevant synaptic plasticity to date.

By fluorescently tagging endogenous GluA1-containing AMPARs and utilizing in vivo two-photon microscopy, we were able to directly visualize the functional strength of endogenous synaptic networks and track how they change during sensory stimulation. We have shown that mechanical stimulation of a single mouse whisker leads to increased synaptic GluA1 specifically in the cortical region corresponding to the

bioRxiv preprint doi: https://doi.org/10.1101/2020.03.01.972216; this version posted March 2, 2020. The copyright holder for this preprint (which was not certified by peer review) is the author/funder. All rights reserved. No reuse allowed without permission.



stimulated whisker. This is consistent with previous studies showing NMDA-receptor-dependent LTP following whisker stimulation (Holtmaat et al., 2009; Zhang et al., 2015). While our proof-of-principle experiments clearly illustrate the power of our approach to image endogenous AMPARs and automatically track synaptic plasticity in vivo, these data represent only the tip of the iceberg. As our genetic labeling strategy illuminates all GluA1-containing synapses throughout the brain, this line enables investigation of synaptic plasticity from any brain region during any behavioral paradigm of interest. Further, this flexible tool is compatible with neuronal activity sensors (e.g. RCaMP), genetic tagging of cell-types of interest (e.g. engram cells, Cre-lines, etc.), and any electrophysiological method. Beyond visualizing fluorescently labeled cortical synapses through cranial windows, one could also use our tools to investigate synaptic dynamics in subcortical structures using cortical excavation, endoscopes, or fiber photometry. More generally, this strategy to directly label endogenous synaptic receptors has several key advantages over previous approaches. Building upon insights gleaned by spine dynamics, in which the formation and elimination of dendritic spines has been shown to be involved in several forms of learning (Holtmaat and Svoboda, 2009; Xu et al., 2009; Yang et al., 2009), our approach additionally enables investigation of plasticity in existing synapses. Recently, similar genetic labeling strategies have been used to investigate other synaptic proteins, such as PSD-95 (Cane et al., 2014; Fortin et al., 2014; Gray et al., 2006; Zhu et al., 2018). These studies have revealed crucial details regarding how scaffolding and structural proteins contribute to dynamic synapse function. Here, we build upon these findings by directly imaging AMPARs, which are the principle functional unit of the synapse. While overexpression of SEP-labeled AMPARs has been previously used to investigate behaviorally relevant plasticity (Diering et al., 2017; Roth et al., 2019; Zhang et al., 2015), the current study is the first to engage labeling of endogenous receptors, which much more faithfully reports the direct physiological mechanisms of plasticity. In future studies, we will expand on our machine-learning approach in order to align, register, and track millions of individual synapses throughout the process of learning.

In conclusion, we aim to fundamentally advance our understanding of the synaptic basis of behavior, moving beyond merely studying synaptic plasticity in single neurons, seeking instead to explore dynamic modulation of the complete synaptome during learning and memory. The tools presented here make this goal achievable.

## Figure Legends

Figure 1. Generation and biochemical characterization of SEP-GluA1 knockin mouse line. **A**. SEP tag was targeted to the extracellular N-terminus, enabling visualization of only functional AMPARs on the cell surface. **B**. Schematic of genetic locus of SEP tag on Exon 1, within the *Gria1* gene encoding GluA1. **C**. Live, confocal image of acute slice of SEP-GluA1. Note the bright fluorescent signal throughout hippocampus and neocortex, indicating widespread expression of SEP-labeled GluA1-containing AMPARs. Age- and coronal-region-matched WT tissue was imaged with the same laser power and presented with identical contrast as SEP-GluA1. **D**. Representative Northern blot of mRNA expression of WT and SEP-GluA1 knockin (KI) mice. SEP-GluA1 is noticeably larger than WT GluA1, due to the inclusion of the SEP tag. **E-F**.

bioRxiv preprint doi: https://doi.org/10.1101/2020.03.01.972216; this version posted March 2, 2020. The copyright holder for this preprint (which was not certified by peer review) is the author/funder. All rights reserved. No reuse allowed without permission.



Representative Western blot and quantification of AMPA receptors expression in the P2 and postsynaptic density (PSD) fractions of WT and SEP-GluA1 mice. GluA1 expression is reduced relative to WT (n=7; *p<0.0001, Student's T-test).

Figure 2. Normal synaptic physiology and receptor trafficking in SEP-GluA1 knockin mice. **A-E**. Whole-cell voltage-clamp recordings from acute slices of aged-matched wild type (WT) and homozygous SEP-GluA1 knockin (KI) littermates. **A-B**. Representative traces of miniature EPSCs from WT (black) and SEP-GluA1 KI (green) mice. **C**. Quantification of amplitude, frequency, and kinetics of miniature EPSCs. No differences were observed in any electrophysiological parameters between WT and KI mice. N=16 and 18 cells from WT and KI, respectively. Unpaired T-tests were used for all comparisons. Mean ± SEM. mEPSC amplitude: WT 9.43±0.20, N=16; KI 10.26±0.51, N=18; P>0.05. Frequency: WT 0.33±0.02; KI 0.33±0.03122; P>0.05. Rise time: WT 2.46±0.040; KI 2.49±0.07; P>0.05. Tau decay: WT 8.49±0.18; KI 8.83±0.36; P>0.05. **D-E**. No differences in rectification were observed between WT and KI mice. Rectification index is the negative slope of the IV curve (between -10 and -60 mV) divided by the positive slope (between +10 and +50 mV). Mean ± SEM. WT: 1.32±0.048, N=12; KI: 1.33±0.042, N=16; P>0.05. **F-G**. Confocal images of cultured SEP-GluA1 neurons stained with antibodies for PSD-95 (F) and c-terminal-GluA1 (G). **H-I**. Quantification of overlap between endogenous SEP-GluA1 signal and immunofluorescence. A significant correlation is observed between the fluorescent intensity of endogenous SEP and the immunofluorescent signal of both PSD-95 (r=0.39, p<0.01, Pearson correlation, n=54 spines) and GluA1 (r=0.49, p<0.001, Pearson correlation, n=60 spines). Lines represent linear regression with 95% confidence interval (dashed lines).

Figure 3. Normal homeostatic and Hebbian plasticity in SEP-GluA1 knockin mice. **A**. Representative Western blot of surface GluA1, GluA2, and GluA3 in WT and KI mouse neurons under baseline conditions, following homeostatic downscaling in bicuculine (Bic), and following homeostatic upscaling in TTX. **B**. Bar plot of all homeostatic plasticity experiments (n=7; *p<0.05, **p<0.01, ***p<0.001; One-way ANOVA). **C**. Induction of long-term potentiation (LTP) in WT and SEP-GluA1 KI mice. Left: fluorescent image depicting experimental setup. CA1 pyramidal neurons were patched and filled with Alexa-594. A stimulating electrode in *stratum radiatum* was used to evoke EPSCs. After recording baseline EPSCs for at least 5 minutes, a pairing protocol consisting of 200 pulses was delivered at 2 Hz. **D.** Average EPSC amplitude normalized to baseline for WT (black) and KI (green) littermates over course of LTP induction. Inset: Example traces of EPSCs from baseline (black) and 30-40 minutes following LTP induction (WT, grey and KI green). **E.** Average change in EPSC amplitude normalized to the baseline period for WT (black) and KI (green) littermates. A significant potentiation of EPSC amplitude was observed in both WT and KI mice, which was not different between genotypes, indicating normal induction and expression of LTP in SEP-GluA1 KI mice. Unpaired T-tests were used for all comparisons. Mean ± SEM. WT: 1.656±0.1673, N=8; KI: 1.594±0.3373, N=8; P>0.05.

Figure 4. Normal behavior in SEP-GluA1 knockin mice. **A-B**. SEP-GluA1 mice display normal locomotion. Age-matched, WT (n=18) and homozygous SEP-GluA1 KI (n=16)

bioRxiv preprint doi: https://doi.org/10.1101/2020.03.01.972216; this version posted March 2, 2020. The copyright holder for this preprint (which was not certified by peer review) is the author/funder. All rights reserved. No reuse allowed without permission.



littermates were placed in an open chamber and locomotion was assessed by counting the total number of beam breaks in a 30-minute session. No differences were detected between WT and KI mice (Repeated measures ANOVA; $F_{1,30}$=1.561, P=0.221), between sexes ($F_{1,30}$=1.346, P=0.255), or in a sex*genotype dependent manner ($F_{1,30}$=0.3, P=0.588). **C-D**. SEP-GluA1 mice display normal anxiety. WT (n=18) and KI (n=16) littermates were placed in an elevated plus maze and anxiety was assessed by measuring the time spent in the open arm. For representative WT and KI animals, time spent in a particular location is indicated in pseudo color, with warm colors indicating higher occupancy. No differences were detected between WT and KI mice (ANOVA; $F_{1,30}$=1.545, P=0.224), between sexes ($F_{1,30}$=0.160, P=0.692), or in a sex*genotype dependent manner ($F_{1,30}$=4.139, P=0.051). **E-F**. SEP-GluA1 mice display normal short-term spatial memory. Spatial novelty preference was assessed in WT (n=18) and KI (n=16) littermates using a Y-maze. WT and KI mice showed a preference for exploration of the novel arm. For representative WT and KI animals, time spent in a particular location is indicated in pseudo color, with warm colors indicating higher occupancy. There was no differences in the time preference ratio (time in novel arm/(time in novel arm + time in familiar arm)) between genotypes (ANOVA; $F_{1,30}$=0.004, P=0.951), between sexes ($F_{1,30}$=1.277, P=0.267), or in a sex*genotype dependent manner ($F_{1,30}$=2.434, P=0.129). Dotted line indicates chance level performance.

Figure 5. SEP intensity correlates with functional synaptic strength. **A**. Two-photon image of a cultured SEP-GluA1 neuron filled with Alexa 594 via somatic patch pipette, imaged at 910nm, with locations of glutamate uncaging indicated as blue dots and manually identified dendritic spines circled in yellow. **B**. Representative uncaging-evoked EPSC (uEPSC) following 1ms pulse of 730nm light at 20mW (blue dot) in 2.5mM MNI-glutamate. **C**. Significant linear correlation between SEP-GluA1 intensity and uEPSC amplitude. SEP-GluA1 intensity was defined as the sum of green fluorescence intensity within manual synaptic annotations from 5 adjacent 0.5µm-spaced z-planes. n=155 spines from 21 cells (*p<0.05, Pearson's chi-squared test). To minimize variability in uEPSC amplitude from electrotonic filtering, all uncaging locations were onto spines on secondary dendrites branching off the primary apical dendrite, with a branch point between 60-110µm from the soma. **D-F**. Tracking synaptic plasticity with SEP-GluA1 in vitro. **D**. Plots of SEP-GluA1 intensity and uEPSC amplitude 5 minutes before and 30 minutes after delivery of an LTP induction stimulus consisting of high-frequency pairing of glutamate uncaging (30 pulses at 0.5 Hz, 1ms pulse of 730nm laser) and postsynaptic depolarization (0mV for 0.5 sec, beginning concurrently with uncaging pulse). Spines that received this LTP stimulus are presented in red (n=10) and spines that did not receive this stimulus are presented in black (n=42). *p<0.01 using one-way ANOVA. **E**. Longitudinal images of the two indicated spines in panel A that received either the LTP induction stimulus (red star) or control (gray star). **F**. Representative uEPSCs during the baseline period (-5 min) and 30 minutes after LTP induction.

Figure 6. Visualizing SEP-GluA1 synapses in vivo using two-photon microscopy. **A**. Schematic of two-photon (2P) in vivo imaging. **B**. Left, single in vivo imaging plane displaying raw, unprocessed SEP-GluA1 signal, taken 47µm deep in layer 1 (L1) of

bioRxiv preprint doi: https://doi.org/10.1101/2020.03.01.972216; this version posted March 2, 2020. The copyright holder for this preprint (which was not certified by peer review) is the author/funder. All rights reserved. No reuse allowed without permission.



barrel cortex. Putative GluA1-containing synapses are identified as bright puncta. Manual synaptic annotations are overlaid as magenta ovals. Right, same cortical plane, but with automatically identified and segmented synapses rendered in arbitrary colors. Manual annotations are overlaid, recolored either green or magenta, corresponding to true positives (defined as >50% of total 3d voxels shared between manual and automatic annotations) or false negative (defined as manual annotations that did not overlap with an automatic detection), respectively; false positives (defined as automatically detected synapses that did not overlap with a manual annotation) are indicated by an X. Scale bar is 1μm. **C**. Large field-of-view imaging plane with overlaid automatic detections, depicting large-scale automatic synapse detection and segmentation, which are rendered as arbitrary colors. Dark areas likely correspond to either vasculature or cell bodies. **D**. Single imaging plane of L1 barrel cortex, showing SEP-GluA1 synapses (green) and a single layer 2/3 pyramidal cell filled with tdTomato (magenta). White arrow denotes a spine devoid of SEP-GluA1 signal. **E**. SEP-GluA1 is enriched in dendritic spines. 66% of automatically detected dendritic spines (visualized using a sparse tdTomato cell fill) contained a SEP-GluA1 synapse, defined as edge-to-edge separation of red spines and green puncta <0.25 μm. This overlap occurred at a substantially higher than chance, as the distance between spines (red channel) and their nearest SEP neighbor (green channel) increased dramatically when the red channel was rotated relative to green (n=504 spines; $p<0.001$; Mann-Whitney U test, relative to unrotated). **F**. GluA1-containing synapses were uniformly detected throughout L1 barrel cortex, up to a depth of 100 μm below the pia surface.

Figure 7. Tracking synaptic plasticity during sensory experience. **A**. Schematic of whisker stimulation and in vivo imaging of barrel cortex. The control unstimulated (D3) and stimulated barrel (C2) were imaged twice at baseline. The C2 whisker was mechanically stimulated with 10 Hz vibration for 1 hour, after which imaging of both barrels resumed. **B-C**. Distribution of normalized SEP-GluA1 intensity in barrel cortex over time in one representative homozygous SEP-GluA1 mouse. **B**. Left: distribution of SEP-GluA1 intensity was stable over time in the control, unstimulated D3 barrel. Right: significant rightward shift in SEP-GluA1 intensity in the C2 barrel following whisker stimulation, indicating net synaptic potentiation. **C**. Split-violin plots depicting distribution of synaptic weights in the control (D3, black) and stimulated (C2, red) barrel during baseline (0 and 1 hours, pooled) and following C2 whisker stimulation (2 and 3 hours, pooled). White or black dots indicate the median SEP-GluA1 intensity. For both B and C, $^{**}p<0.01$, Mann-Whitney U test relative to within-mouse baseline period (pooled 0 and 1 hour timepoints). **D**. Whisker-stimulation induces barrel-selective synaptic potentiation. Plot of mean SEP-GluA1 fluorescent intensity from all automatically detected SEP puncta over time in the control (black, D3) and stimulated (red, C2) barrel. n=4 mice, $^{**}p<0.01$, 2-way ANOVA. Error bars represent standard deviation. **E**. Whisker-stimulation induces barrel-selective synapse enlargement. Plot of mean area of all automatically detected SEP puncta over time in the control (black, D3) and stimulated (red, C2) barrel. Synapse area was defined as the maximum area in a single 2d imaging plane for each automatically segmented SEP-GluA1 puncta. $^{*}p<0.05$, 2-way ANOVA. **F**. Number of detected synapses was stable over time. Total synapse count from each individual mouse (grey) and mean (n=4, black) are presented.

bioRxiv preprint doi: https://doi.org/10.1101/2020.03.01.972216; this version posted March 2, 2020. The copyright holder for this preprint (which was not certified by peer review) is the author/funder. All rights reserved. No reuse allowed without permission.



## Methods and Materials

*Neuronal culture*

Mouse embryonic (E18) cortical/hippocampal neurons were plated on poly-L-lysine coated tissue culture dishes/glass coverslips at a density of 65,000 cells/cm$^2$/37,500 cells/cm$^2$ in NM5 medium (neurobasal media (Invitrogen) supplemented with 2% B-27, 2 mM Glutamax, 50 U/mL PenStrep, and 5% horse serum (Invitrogen)) and grown in NM0 medium (neurobasal media (Invitrogen) supplemented with 2% B-27, 2 mM Glutamate, 50 U/mL PenStrep). Cultured cortical neurons/hippocampal neurons were fed twice/once per week. To induce synaptic scaling, cortical neurons were treated with bicuculline (20 µM) or tetrodotoxin (TTX, 1 µM) at DIV 11-13 for 48 hours. Hippocampal neurons were used at DIV 19-22 for glutamate uncaging.

*Surface biotinylation*

Neurons were rinsed with ice-cold PBSCM (1 × PBS, 1mM $MgCl_2$, 0.1mM $CaCl_2$, pH 8.0) once and then incubated with Sulfo-NHS-SS-biotin (0.5mg/ml, Thermo Scientific) for 30 minutes at 4°C. Residual unreacted biotinylation reagent was washed out with PBSCM and quenched by 20mM glycine twice for 5 minutes. Neurons were lysed in lysis buffer [PBS containing 50mM NaF, 5mM sodium pyrophosphate, 1% NP-40, 1% sodium deoxycholate, 0.02% SDS, and protease inhibitor cocktail (Roche)]. 20 µg lysates were incubated overnight with NeutraAvidin agarose beads (Thermo Scientific) and then were washed with lysis buffer four times. Biotinylated proteins were eluted using 2× SDS loading buffer. Surface proteins were then subjected to SDS-PAGE and analyzed by western blot.

*PSD fractionation*

Mouse hippocampus tissues were homogenized in buffer [320mM sucrose, 5mM sodium pyrophosphate, 1mM EDTA, 10mM HEPES pH 7.4, 200nM okadaic acid, protease inhibitor cocktail (Roche)] using a 26-gauge needle. Homogenate was centrifuged at 800 × g for 10 minutes at 4°C to yield P1 and S1. S1 was centrifuged at 20,000 × g for 20 minutes to yield P2 and S2. P2 was then resuspended in water adjusted to 4mM HEPES pH 7.4 followed by 30 minutes' agitation at 4°C. Suspended P2 was centrifuged at 25,000 × g for 20 minutes at 4°C. The resulted pellet was resuspended in 50mM HEPES pH 7.4, mixed with an equal volume of 1% triton X-100, and agitated at 4°C for 10 minutes. The PSD fraction was generated by centrifugation at 32,000 x g for 20 minutes at 4°C.

*Immunohistochemistry and confocal imaging*

Cultured hippocampal neurons were fixed for 20 min in PBS containing 4% paraformaldehyde (PFA)/4% sucrose, rinsed with PBS, and permeabilized for 10 min with 0.2% Triton X-100. Neurons were blocked with 1% bovine serum albumin (BSA) in PBS for 60 min at 37°C before incubation with primary antibodies in PBS containing 0.3% BSA for at 4°C overnight. Coverslips were washed with PBS before the neurons were incubated with secondary antibodies in PBS containing 0.3% BSA for 1h at room temperature. After washing with PBS and water, coverslips were mounted onto glass

bioRxiv preprint doi: https://doi.org/10.1101/2020.03.01.972216; this version posted March 2, 2020. The copyright holder for this preprint (which was not certified by peer review) is the author/funder. All rights reserved. No reuse allowed without permission.



slides using Permafluor (Fischer Scientific). Images were obtained using an LSM880 laser scanning confocal microscope (Zeiss). The following antibodies were used: anti-GluA1 C-terminal pAb (JH4294, made in house), anti-PSD95 mAb (NeuroMab), anti-GFP pAb (GFP-1010, Aves Labs, Inc), anti-dsRed2 (Clontech), Alexa Fluor 488 goat anti-chicken (Thermo Fisher Scientific), Alexa Fluor 568 goat anti-rabbit (Thermo Fisher Scientific), and Alexa Fluor 647 goat anti-rat (Thermo Fisher Scientific).

*Electrophysiological recordings*

Whole-cell voltage-clamp recordings were performed in CA1 pyramidal neuron of acute hippocampal slices from 3-4-weeks-old paired littermates of mice by an experimenter blind to genotype. Slices were prepared in ice-cold oxygenated dissection buffer containing the following (in mM):210 Sucrose, 7 Glucose, 26.2 $NaHCO_3$, 2.5 KCl, 1 $NaH_2PO_4$, $7MgSO_4$. For all recordings, slices were perfused in ACSF (119mM NaCl, 26.2 mM $NaHCO_3$ and 11 mM glucose, 2.5 mM KCl, 1 mM $NaH_2PO_4$, 2.5 mM $CaCl_2$, 1.3 mM $MgSO_4$, 50-100µM Picrotoxin) at room temperature. Neurons were patched by glass pipettes (3-5 MΩ) which were filled with internal solution (115 mM Cs-$MeSO_3$, 0.4 mM EGTA, 5 mM TEA-Cl, 2.8 mM NaCl, 20 mM HEPES, 3 mM Mg-ATP, 0.5 mM $Na_2$-GTP, 10 mM Na Phosphocreatine, 5 mM QX-314). mEPSC recordings were performed in the ACSF in presence of 1µM TTX, and cells were hold at -70mV. Data from 5-10 min after break-in were used for mEPSC analysis. For rectification and LTP experiments, EPSCs were elicited at 0.1 Hz by electrical stimulation (0.1 ms, 8-20 µA) via a stimulating electrode positioned in stratum radiatum. During rectification measurements, cells were hold at -60 to 60 mV before liquid junction modification. Each data point at each potential was averaged by 5-10 EPSCs. LTP was induced by a train of 200 pulses at 2 Hz paired with 0 mV depolarization. Data are presented as EPSC amplitude averaged at 1-min intervals and then normalized to the average of baseline response. Signals were measured with MultiClamp 700B amplifier and digitized at 10kHz by using a Digidata 1440A. Data acquisition were performed with pClamp 10.5 software. Access resistance (Ra) was monitored throughout the recording. Cells in which the Ra > 20 MΩ or Ra varied by more than 20% were discarded.

*Mouse behavior*

Behavioral testing was performed in homozygous SEP-GluA1 mice (9 females and 7 males) and WT (9 females and 9 males) littermate controls, aged 6-10 weeks. Animals were housed in a holding room on a reverse light cycle, and testing was conducted during the dark (i.e. active) phase.

Locomotor activity was assessed by placing animals in an illuminated open arena (40x40cm) and measuring the number of infrared beam breaks during a 30-minute session (San Diego Instruments Inc.). Anxiety was assessed using an elevated plus maze (66cm long and 5cm wide; San Diego Instruments Inc.), consisting of two closed arms and two open arms suspended 54cm above the ground. Immediately before testing, animals were placed, individually, into a clean cage for 5 minutes. Animals were placed onto the center of the elevated plus maze facing an open arm and allowed to explore for 5 minutes. The position of the animal was tracked with using ANYmaze software (Stoelting).

bioRxiv preprint doi: https://doi.org/10.1101/2020.03.01.972216; this version posted March 2, 2020. The copyright holder for this preprint (which was not certified by peer review) is the author/funder. All rights reserved. No reuse allowed without permission.



Spatial short-term memory was assessed by testing spatial novelty preference using a Y maze. The Y-maze was made of clear plexiglass (each arm 38cm long; San Diego Instruments Inc.) and surrounded by distal spatial cues. A mixture of clean and dirty sawdust (ratio 2:1) was added to the bottom of the maze to promote exploration of the maze. The dirty sawdust was collected from other cages mice, of the same sex as the animals being tested. Immediately before testing, animals were placed, individually, into a clean cage for 5 minutes. The test was split into exposure and test phases. During the exposure phase, one of the Y-maze arms was blocked (counterbalanced for genotype) and animals were allowed to explore two arms of the maze for 5 minutes. After this exposure phase, animals were gently removed from the maze and returned to the temporary holding cage for 1 minute. During which the sawdust was re-distributed and all arms of the maze were made available. For the test phase, mice were re-exposed to the maze and allowed to explore all arms for 2 minutes. The position of the animal was tracked with using ANYmaze software (Stoelting). Testing was conducted by an experimenter blind to genotype of the mice being tested. Statistical comparisons were made using SPSS(IBM). Sex and genotype were used as between subject variables.

*Glutamate-uncaging*

Cultured mouse cortical neurons (10:1 mixture of WT and homozygous SEP-GluA1) were plated at E18 and imaged on DIV 16-18. Neurons were perfused in a modified HEPES-based ACSF solution, consisting of (in mM): 140 NaCl, 5 KCl, 10 glucose, 10 HEPES, 2 $CaCl_2$, 1 $MgCl_2$, 1 TTX, and 2.5 mM MNI-caged-L-glutamate (Tocris), pH=7.30 and 310-316 mOsm. Recordings were made at room temperature in recirculated ACSF (3 mL/min). Recording pipettes were fabricated (Flaming/Brown Micropipette Puller, Sutter Instruments) from borosilicate capillary glass (Sutter, 4–6 MΩ open-tip resistance) and filled with (in mM): 115 CsMeSO4, 2.8 NaCl, 5 TEACl, 0.4 EGTA, 20 HEPES, 3 MgATP, 0.5 NaGTP, 10 NaPhosphocreatine, and 2.5 QX-314, pH = 7.32 and 306 mOsm, and containing a 1% Alexa-594 dye (Tocris). Whole-cell voltage-clamp recordings were made using a MultiClamp 700B amplifier and Digidata 1440A digitizer (Axon Instruments).

Neurons were imaged with a 20X/1.0 NA water-immersion objective (Zeiss) and a custom-built two-photon microscope controlled by ScanImage (Vidrio Technologies, Ashburn, VA). Dendritic morphology was visualized using an Alexa dye, delivered by the patch pipette). SEP-GluA1 and red cell fill were excited at 910 nm using a tunable Ti:sapphire laser (Coherent, Santa Clara, CA). Images were acquired at 1024x1024 resolution and slices within z-stacks spaced every 0.5 µm. A second two-photon laser (Spectra Physics, Santa Clara, CA) was used to uncage glutamate (1 ms pulse) onto visually identified spines at a wavelength of 730 nm and a power of 20 mW at the objective back aperture. Uncaging position was controlled using custom software developed in our lab (Scan Stim™ by Dr. Ingie Hong). The offset between the imaging and uncaging two-photon lasers was directly measured and corrected on a monthly basis. To measure the glutamate-uncaging-evoked excitatory postsynaptic current (uEPSC), we used pClamp (Axon Instruments) to synchronize triggering of the uncaging laser with voltage-clamp recordings. To minimize the effect of electrotonic filtering caused by variable numbers of branch points between the site of dendritic uncaging and

bioRxiv preprint doi: https://doi.org/10.1101/2020.03.01.972216; this version posted March 2, 2020. The copyright holder for this preprint (which was not certified by peer review) is the author/funder. All rights reserved. No reuse allowed without permission.



the somatic recording pipette, we uncaged exclusively onto spines of secondary dendrites, located 95-160 µm from the cell body. We uncaged on 4-8 spines/dendritic segment and 1-3 dendritic segments/neuron. To quantify the SEP-GluA1 and cell-fill signals, we manually drew ROIs around visually identified spines, summed the fluorescent intensity of five adjacent Z-sections (each separated by 0.5 µm), and subtracted size-matched neighboring background ROIs. Representative images shown in figures were median filtered and contrast enhanced. The uncaging-LTP-induction stimulus consisted of 30 pairings of glutamate uncaging (1ms pulse of 730nm laser at 0.5 Hz) and postsynaptic depolarization (0mV for 0.5 sec, beginning concurrently with uncaging pulse). Spines were imaged every 5 minutes and synaptic strength was probed by measuring the uEPSC amplitude of each identified spine every 1 minute.

*Cranial window surgery and viral injection*

Mice were anesthetized (2% isoflurane) and implanted with a 3x3 mm cranial window (Potomac Photonics) over the barrel cortex region of somatosensory cortex at 2-3 months of age. Windows were sealed and custom-made metal head bars attached using dental cement (Metabond; Edgewood, NY). In a subset of experiments, an AAV-CaMKII-cre virus (Addgene/Penn Vector) was injected into barrel cortex (1:10k-1:50k dilution, 100-150 nL, 0.3 mm deep) of double homozygous SEP-GluA1 x Ai9 reporter mice to sparsely label L2/3 pyramidal neurons with a tdTomato (red) cell fill. 10 mg/kg of extended release Buprenorphine (ZooPharm) was administered before surgery and mice were observed for 3 days following surgery. Mice were allowed to recover from surgery for at least 2 weeks before commencing in vivo imaging. All surgical procedures were approved by the Johns Hopkins Johns Hopkins Animal Care and Use Committee.

*Cranial window surgery and viral injection*

Mice were anesthetized (2% isoflurane) and implanted with a 3x3 mm cranial window (Potomac Photonics) over the barrel cortex region of somatosensory cortex at 2-3 months of age. Windows were sealed and custom-made metal head bars attached using dental cement (Metabond; Edgewood, NY). In a subset of experiments, an AAV-CaMKII-cre virus (Addgene/Penn Vector) was injected into barrel cortex (1:10k-1:50k dilution, 100-150 nL, 0.3 mm deep) of double homozygous SEP-GluA1 x Ai9 reporter mice to sparsely label L2/3 pyramidal neurons with a tdTomato (red) cell fill. 10 mg/kg of extended release Buprenorphine (ZooPharm) was administered before surgery and mice were observed for 3 days following surgery. Mice were allowed to recover from surgery for at least 2 weeks before commencing in vivo imaging. All surgical procedures were approved by the Johns Hopkins Johns Hopkins Animal Care and Use Committee.

*Optical-intrinsic and in vivo two-photon imaging*

Optical intrinsic imaging was used to map select barrels within somatosensory cortex as previously described (Zhang et al., 2015). Briefly, we mechanically stimulated the individual C2 and D3 whiskers using a custom-built piezo driver at 10Hz and used optical intrinsic imaging to identify the corresponding barrel fields. Mice were anesthetized and maintained on 0.5% isoflurane supplemented by xylazine (13 mg/kg). Optical images of barrel cortex were acquired at 30 Hz using a CCD camera (Grasshopper GS3-U3-23S6M-C under red LED light (630 nm) with a 2.5×/0.075

bioRxiv preprint doi: https://doi.org/10.1101/2020.03.01.972216; this version posted March 2, 2020. The copyright holder for this preprint (which was not certified by peer review) is the author/funder. All rights reserved. No reuse allowed without permission.



numerical aperture (NA) objective (Zeiss). Images were collected, averaged (across 30 trials), Gaussian filtered ($\sigma$ = 10 µm), and baseline subtracted. Widefield images of both barrels were acquired and vasculature was used to align subsequent two-photon imaging of the same regions.

Two-photon in vivo images were acquired from lightly anesthetized mice (13 mg/kg xylazine and 0.5% isoflurane) using a custom-built, two-photon laser-scanning microscope controlled by ScanImage (Vidrio, Ashburn, VA) and a 20×/1.0 NA water-immersion objective lens (Zeiss). SEP-GluA1 (green) and tdTomato cell fill (red) were both excited at 910 nm with a Ti:sapphire laser (Coherent, 20 mW of power delivered to the objective back-aperture). Green and red fluorescence signals were acquired simultaneously and separated by a set of dichroic mirrors (MOM system, Sutter Instrument) and filters (ET525/50m for green channel, ET605/70m for red channel, Chroma). Image stacks were acquired at 1,024 × 1,024 pixels with a voxel size of 0.089 µm in XY, with a z-step of 1 µm. Representative images shown in figures were median filtered (1 pixel radius) and contrast enhanced.

*Automatic synapse detection and segmentation*

To automatically detect SEP-labeled synapses, we used a Weiner filtering method, employing pre-whitened matched templates based on the mean appearance of conspicuous fluorescent puncta and background noise. Inhomogeneity due to nonuniform illumination was corrected using cubic polynomial detrending on each slice, followed by quadratic polynomial detrending of the 3d volume. Regions lacking detectable SEP fluorescence, such as blood vessels and cell bodies, were excluded by thresholding. To convert each individual synapse to a unique label, region growing techniques were used, starting at local maxima, rather than using a traditional watershed approach. To be detected, puncta were required to have above-threshold signal intensity (dynamically set relative to background) in at least 10 voxels, but no more than 150 voxels, with a voxel size of 0.089 x 0.089 x 1.0 µm in XYZ. Puncta with total fluorescence below threshold or volumes outside of this range were excluded. Handling these large datasets was addressed by storing individual synapse labels in a KD tree, thereby enabling efficient querying neighborhoods, while splitting versus joining were optimized using farthest-first traversals. This approach enabled flexibility to tune segmentations based on accuracy criteria, such as tradeoffs between sensitivity and specificity, as well as prior information about synapse size and shape.

bioRxiv preprint doi: https://doi.org/10.1101/2020.03.01.972216; this version posted March 2, 2020. The copyright holder for this preprint (which was not certified by peer review) is the author/funder. All rights reserved. No reuse allowed without permission.



## References

Andersen, P., Sundberg, S.H., Sveen, O., and Wigstrom, H. (1977). Specific long-lasting potentiation of synaptic transmission in hippocampal slices. Nature *266*, 736-737.

Anggono, V., and Huganir, R.L. (2012). Regulation of AMPA receptor trafficking and synaptic plasticity. Curr Opin Neurobiol *22*, 461-469.

Araki, Y., Zeng, M., Zhang, M., and Huganir, R.L. (2015). Rapid dispersion of SynGAP from synaptic spines triggers AMPA receptor insertion and spine enlargement during LTP. Neuron *85*, 173-189.

Ashby, M.C., De La Rue, S.A., Ralph, G.S., Uney, J., Collingridge, G.L., and Henley, J.M. (2004). Removal of AMPA receptors (AMPARs) from synapses is preceded by transient endocytosis of extrasynaptic AMPARs. J Neurosci *24*, 5172-5176.

Bannerman, D.M., Deacon, R.M., Brady, S., Bruce, A., Sprengel, R., Seeburg, P.H., and Rawlins, J.N. (2004). A comparison of GluR-A-deficient and wild-type mice on a test battery assessing sensorimotor, affective, and cognitive behaviors. Behav Neurosci *118*, 643-647.

Berryer, M.H., Hamdan, F.F., Klitten, L.L., Moller, R.S., Carmant, L., Schwartzentruber, J., Patry, L., Dobrzeniecka, S., Rochefort, D., Neugnot-Cerioli, M.*, et al.* (2013). Mutations in SYNGAP1 cause intellectual disability, autism, and a specific form of epilepsy by inducing haploinsufficiency. Hum Mutat *34*, 385-394.

Bhatt, D.H., Zhang, S., and Gan, W.B. (2009). Dendritic spine dynamics. Annu Rev Physiol *71*, 261-282.

Bittner, K.C., Milstein, A.D., Grienberger, C., Romani, S., and Magee, J.C. (2017). Behavioral time scale synaptic plasticity underlies CA1 place fields. Science *357*, 1033-1036.

Bliss, T.V., and Lomo, T. (1973). Long-lasting potentiation of synaptic transmission in the dentate area of the anaesthetized rabbit following stimulation of the perforant path. J Physiol *232*, 331-356.

Boerner, T., Bygrave, A.M., Chen, J., Fernando, A., Jackson, S., Barkus, C., Sprengel, R., Seeburg, P.H., Harrison, P.J., Gilmour, G.*, et al.* (2017). The group II metabotropic glutamate receptor agonist LY354740 and the D2 receptor antagonist haloperidol reduce locomotor hyperactivity but fail to rescue spatial working memory in GluA1 knockout mice. Eur J Neurosci *45*, 912-921.

Bygrave, A.M., Jahans-Price, T., Wolff, A.R., Sprengel, R., Kullmann, D.M., Bannerman, D.M., and Katzel, D. (2019). Hippocampal-prefrontal coherence mediates working memory and selective attention at distinct frequency bands and provides a causal link between schizophrenia and its risk gene GRIA1. Transl Psychiatry *9*, 142.

Cane, M., Maco, B., Knott, G., and Holtmaat, A. (2014). The relationship between PSD-95 clustering and spine stability in vivo. J Neurosci *34*, 2075-2086.

bioRxiv preprint doi: https://doi.org/10.1101/2020.03.01.972216; this version posted March 2, 2020. The copyright holder for this preprint (which was not certified by peer review) is the author/funder. All rights reserved. No reuse allowed without permission.



Diaz-Alonso, J., Sun, Y.J., Granger, A.J., Levy, J.M., Blankenship, S.M., and Nicoll, R.A. (2017). Subunit-specific role for the amino-terminal domain of AMPA receptors in synaptic targeting. Proc Natl Acad Sci U S A *114*, 7136-7141.

Diering, G.H., Nirujogi, R.S., Roth, R.H., Worley, P.F., Pandey, A., and Huganir, R.L. (2017). Homer1a drives homeostatic scaling-down of excitatory synapses during sleep. Science *355*, 511-515.

Dombeck, D.A., Harvey, C.D., Tian, L., Looger, L.L., and Tank, D.W. (2010). Functional imaging of hippocampal place cells at cellular resolution during virtual navigation. Nat Neurosci *13*, 1433-1440.

El-Boustani, S., Ip, J.P.K., Breton-Provencher, V., Knott, G.W., Okuno, H., Bito, H., and Sur, M. (2018). Locally coordinated synaptic plasticity of visual cortex neurons in vivo. Science *360*, 1349-1354.

Epsztein, J., Brecht, M., and Lee, A.K. (2011). Intracellular determinants of hippocampal CA1 place and silent cell activity in a novel environment. Neuron *70*, 109-120.

Fenno, L., Yizhar, O., and Deisseroth, K. (2011). The development and application of optogenetics. Annu Rev Neurosci *34*, 389-412.

Fortin, D.A., Tillo, S.E., Yang, G., Rah, J.C., Melander, J.B., Bai, S., Soler-Cedeno, O., Qin, M., Zemelman, B.V., Guo, C.*, et al.* (2014). Live imaging of endogenous PSD-95 using ENABLED: a conditional strategy to fluorescently label endogenous proteins. J Neurosci *34*, 16698-16712.

Frey, U., and Morris, R.G. (1997). Synaptic tagging and long-term potentiation. Nature *385*, 533-536.

Gray, N.W., Weimer, R.M., Bureau, I., and Svoboda, K. (2006). Rapid redistribution of synaptic PSD-95 in the neocortex in vivo. PLoS Biol *4*, e370.

Henley, J.M., and Wilkinson, K.A. (2016). Synaptic AMPA receptor composition in development, plasticity and disease. Nat Rev Neurosci *17*, 337-350.

Holtmaat, A., Bonhoeffer, T., Chow, D.K., Chuckowree, J., De Paola, V., Hofer, S.B., Hubener, M., Keck, T., Knott, G., Lee, W.C.*, et al.* (2009). Long-term, high-resolution imaging in the mouse neocortex through a chronic cranial window. Nat Protoc *4*, 1128-1144.

Holtmaat, A., and Svoboda, K. (2009). Experience-dependent structural synaptic plasticity in the mammalian brain. Nat Rev Neurosci *10*, 647-658.

Holtmaat, A., Wilbrecht, L., Knott, G.W., Welker, E., and Svoboda, K. (2006). Experience-dependent and cell-type-specific spine growth in the neocortex. Nature *441*, 979-983.

Huganir, R.L., and Nicoll, R.A. (2013). AMPARs and synaptic plasticity: the last 25 years. Neuron *80*, 704-717.

Juavinett, A.L., Bekheet, G., and Churchland, A.K. (2019). Chronically implanted Neuropixels probes enable high-yield recordings in freely moving mice. Elife *8*.

bioRxiv preprint doi: https://doi.org/10.1101/2020.03.01.972216; this version posted March 2, 2020. The copyright holder for this preprint (which was not certified by peer review) is the author/funder. All rights reserved. No reuse allowed without permission.



Jun, J.J., Steinmetz, N.A., Siegle, J.H., Denman, D.J., Bauza, M., Barbarits, B., Lee, A.K., Anastassiou, C.A., Andrei, A., Aydin, C.*, et al.* (2017). Fully integrated silicon probes for high-density recording of neural activity. Nature *551*, 232-236.

Kopec, C.D., Li, B., Wei, W., Boehm, J., and Malinow, R. (2006). Glutamate receptor exocytosis and spine enlargement during chemically induced long-term potentiation. J Neurosci *26*, 2000-2009.

Lee, K.F., Soares, C., and Beique, J.C. (2012). Examining form and function of dendritic spines. Neural Plast *2012*, 704103.

Lin, M.Z., and Schnitzer, M.J. (2016). Genetically encoded indicators of neuronal activity. Nat Neurosci *19*, 1142-1153.

Makino, H., and Malinow, R. (2009). AMPA receptor incorporation into synapses during LTP: the role of lateral movement and exocytosis. Neuron *64*, 381-390.

Malinow, R., and Malenka, R.C. (2002). AMPA receptor trafficking and synaptic plasticity. Annu Rev Neurosci *25*, 103-126.

Matsuzaki, M., Ellis-Davies, G.C., Nemoto, T., Miyashita, Y., Iino, M., and Kasai, H. (2001). Dendritic spine geometry is critical for AMPA receptor expression in hippocampal CA1 pyramidal neurons. Nat Neurosci *4*, 1086-1092.

McNaughton, B.L., Douglas, R.M., and Goddard, G.V. (1978). Synaptic enhancement in fascia dentata: cooperativity among coactive afferents. Brain Res *157*, 277-293.

Miesenbock, G., De Angelis, D.A., and Rothman, J.E. (1998). Visualizing secretion and synaptic transmission with pH-sensitive green fluorescent proteins. Nature *394*, 192-195.

Nabavi, S., Fox, R., Alfonso, S., Aow, J., and Malinow, R. (2014). GluA1 trafficking and metabotropic NMDA: addressing results from other laboratories inconsistent with ours. Philos Trans R Soc Lond B Biol Sci *369*, 20130145.

Nicoll, R.A. (2017). A Brief History of Long-Term Potentiation. Neuron *93*, 281-290.

O'Brien, R.J., Kamboj, S., Ehlers, M.D., Rosen, K.R., Fischbach, G.D., and Huganir, R.L. (1998). Activity-dependent modulation of synaptic AMPA receptor accumulation. Neuron *21*, 1067-1078.

Patterson, M.A., Szatmari, E.M., and Yasuda, R. (2010). AMPA receptors are exocytosed in stimulated spines and adjacent dendrites in a Ras-ERK-dependent manner during long-term potentiation. Proc Natl Acad Sci U S A *107*, 15951-15956.

Roth, R.H., Cudmore, R.H., Tan, H.L., Hong, I., Zhang, Y., and Huganir, R.L. (2019). Cortical Synaptic AMPA Receptor Plasticity during Motor Learning. Neuron.

Roth, R.H., Zhang, Y., and Huganir, R.L. (2017). Dynamic imaging of AMPA receptor trafficking in vitro and in vivo. Curr Opin Neurobiol *45*, 51-58.

bioRxiv preprint doi: https://doi.org/10.1101/2020.03.01.972216; this version posted March 2, 2020. The copyright holder for this preprint (which was not certified by peer review) is the author/funder. All rights reserved. No reuse allowed without permission.



Sanderson, D.J., Gray, A., Simon, A., Taylor, A.M., Deacon, R.M., Seeburg, P.H., Sprengel, R., Good, M.A., Rawlins, J.N., and Bannerman, D.M. (2007). Deletion of glutamate receptor-A (GluR-A) AMPA receptor subunits impairs one-trial spatial memory. Behav Neurosci *121*, 559-569.

Sdrulla, A.D., and Linden, D.J. (2007). Double dissociation between long-term depression and dendritic spine morphology in cerebellar Purkinje cells. Nat Neurosci *10*, 546-548.

Sheng, N., Bemben, M.A., Diaz-Alonso, J., Tao, W., Shi, Y.S., and Nicoll, R.A. (2018). LTP requires postsynaptic PDZ-domain interactions with glutamate receptor/auxiliary protein complexes. Proc Natl Acad Sci U S A *115*, 3948-3953.

Sofroniew, N.J., Flickinger, D., King, J., and Svoboda, K. (2016). A large field of view two-photon mesoscope with subcellular resolution for in vivo imaging. Elife *5*.

Spruston, N. (2008). Pyramidal neurons: dendritic structure and synaptic integration. Nat Rev Neurosci *9*, 206-221.

Trachtenberg, J.T., Chen, B.E., Knott, G.W., Feng, G., Sanes, J.R., Welker, E., and Svoboda, K. (2002). Long-term in vivo imaging of experience-dependent synaptic plasticity in adult cortex. Nature *420*, 788-794.

Turrigiano, G.G., Leslie, K.R., Desai, N.S., Rutherford, L.C., and Nelson, S.B. (1998). Activity-dependent scaling of quantal amplitude in neocortical neurons. Nature *391*, 892-896.

Volk, L., Chiu, S.L., Sharma, K., and Huganir, R.L. (2015). Glutamate synapses in human cognitive disorders. Annu Rev Neurosci *38*, 127-149.

Xu, N.L., Harnett, M.T., Williams, S.R., Huber, D., O'Connor, D.H., Svoboda, K., and Magee, J.C. (2012). Nonlinear dendritic integration of sensory and motor input during an active sensing task. Nature *492*, 247-251.

Xu, T., Yu, X., Perlik, A.J., Tobin, W.F., Zweig, J.A., Tennant, K., Jones, T., and Zuo, Y. (2009). Rapid formation and selective stabilization of synapses for enduring motor memories. Nature *462*, 915-919.

Yang, G., Pan, F., and Gan, W.B. (2009). Stably maintained dendritic spines are associated with lifelong memories. Nature *462*, 920-924.

Zamanillo, D., Sprengel, R., Hvalby, O., Jensen, V., Burnashev, N., Rozov, A., Kaiser, K.M., Koster, H.J., Borchardt, T., Worley, P.*, et al.* (1999). Importance of AMPA receptors for hippocampal synaptic plasticity but not for spatial learning. Science *284*, 1805-1811.

Zhang, Y., Cudmore, R.H., Lin, D.T., Linden, D.J., and Huganir, R.L. (2015). Visualization of NMDA receptor-dependent AMPA receptor synaptic plasticity in vivo. Nat Neurosci *18*, 402-407.

Zhou, Z., Liu, A., Xia, S., Leung, C., Qi, J., Meng, Y., Xie, W., Park, P., Collingridge, G.L., and Jia, Z. (2018). The C-terminal tails of endogenous GluA1 and GluA2 differentially contribute to hippocampal synaptic plasticity and learning. Nat Neurosci *21*, 50-62.

bioRxiv preprint doi: https://doi.org/10.1101/2020.03.01.972216; this version posted March 2, 2020. The copyright holder for this preprint (which was not certified by peer review) is the author/funder. All rights reserved. No reuse allowed without permission.



Zhu, F., Cizeron, M., Qiu, Z., Benavides-Piccione, R., Kopanitsa, M.V., Skene, N.G., Koniaris, B., DeFelipe, J., Fransen, E., Komiyama, N.H.*, et al.* (2018). Architecture of the Mouse Brain Synaptome. Neuron *99*, 781-799 e710.

bioRxiv preprint doi: https://doi.org/10.1101/2020.03.01.972216; this version posted March 2, 2020. The copyright holder for this preprint (which was not certified by peer review) is the author/funder. All rights reserved. No reuse allowed without permission.

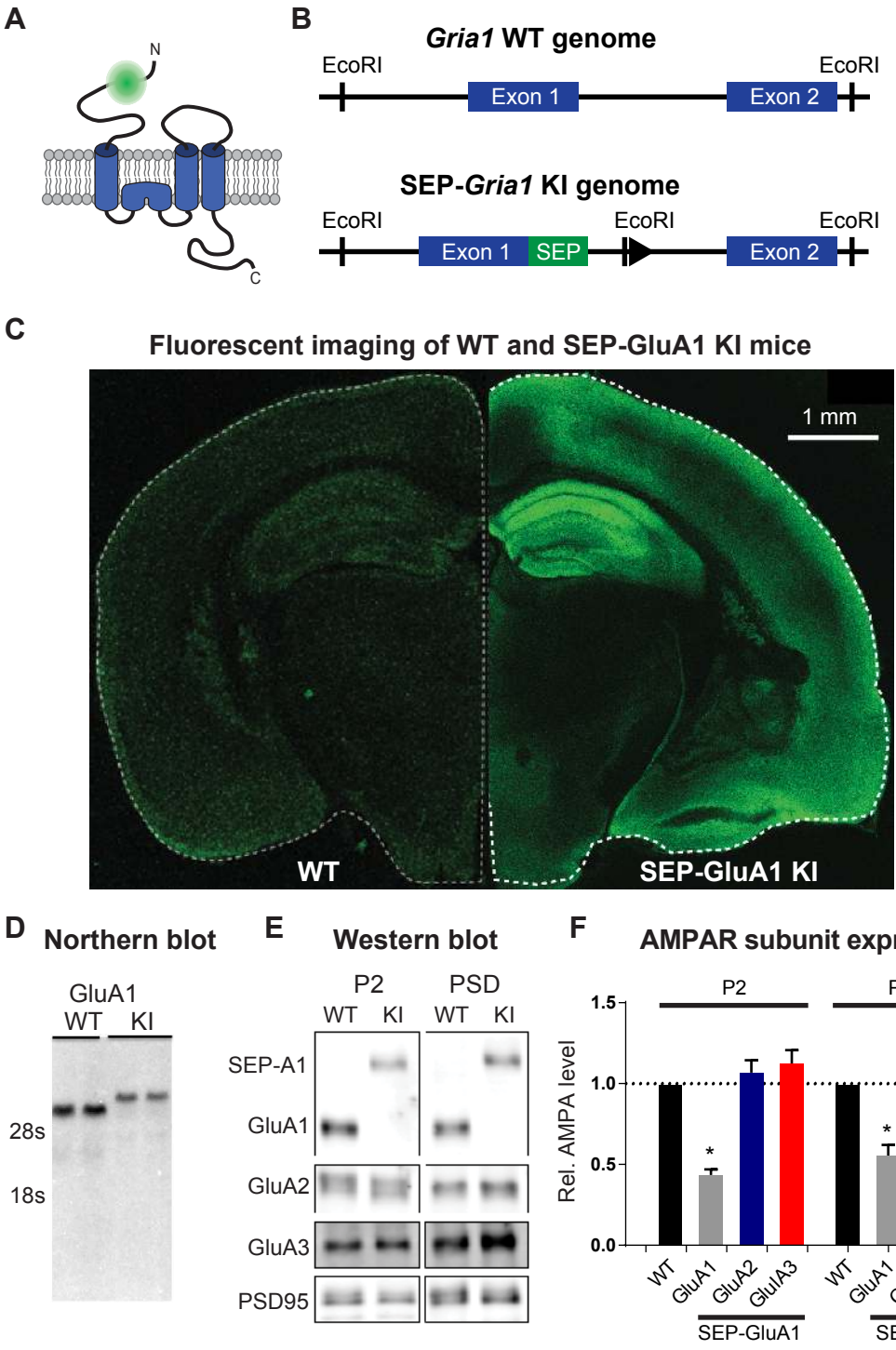


Fig. 1

bioRxiv preprint doi: https://doi.org/10.1101/2020.03.01.972216; this version posted March 2, 2020. The copyright holder for this preprint (which was not certified by peer review) is the author/funder. All rights reserved. No reuse allowed without permission.

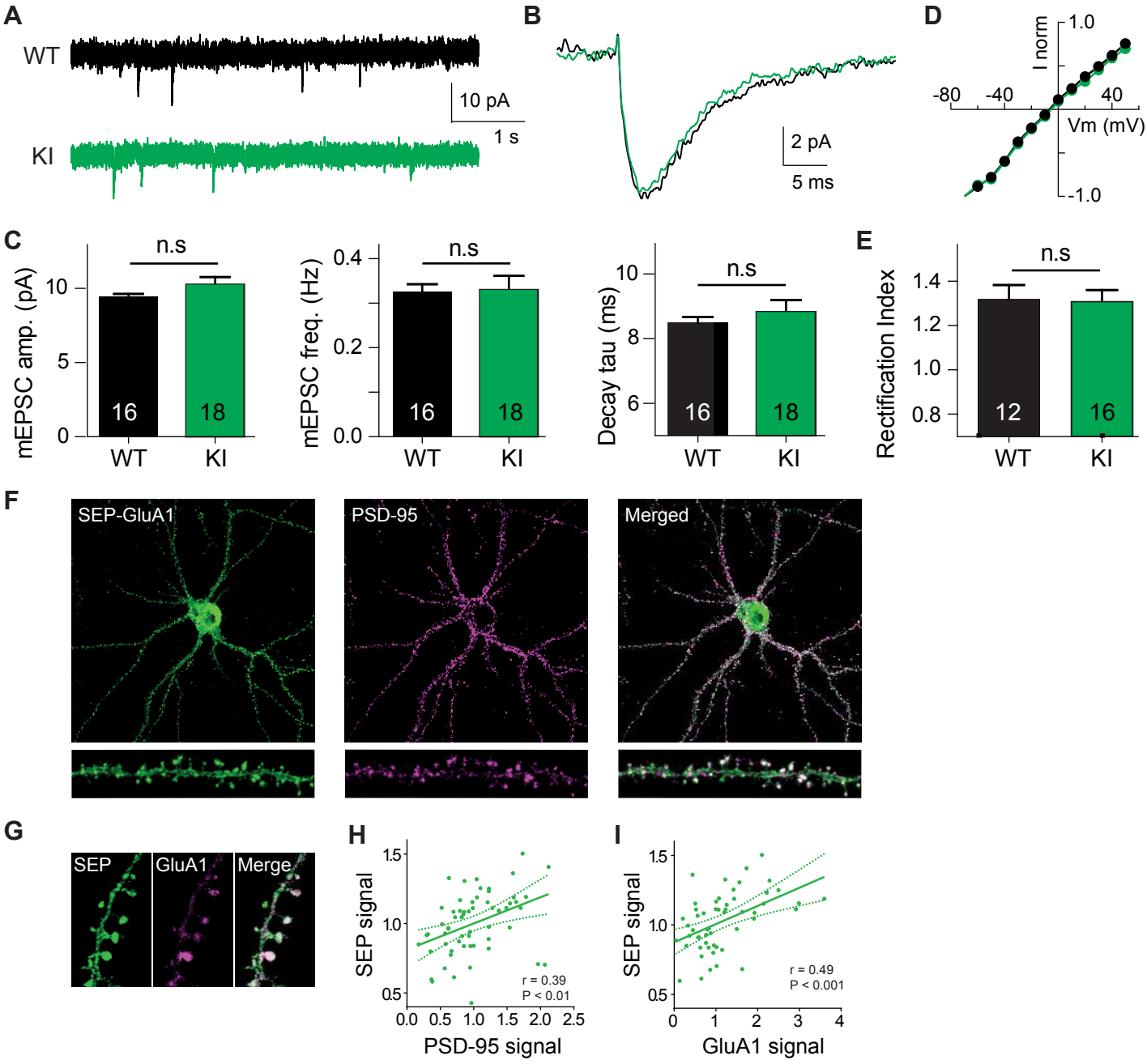


Fig. 2

bioRxiv preprint doi: https://doi.org/10.1101/2020.03.01.972216; this version posted March 2, 2020. The copyright holder for this preprint (which was not certified by peer review) is the author/funder. All rights reserved. No reuse allowed without permission.

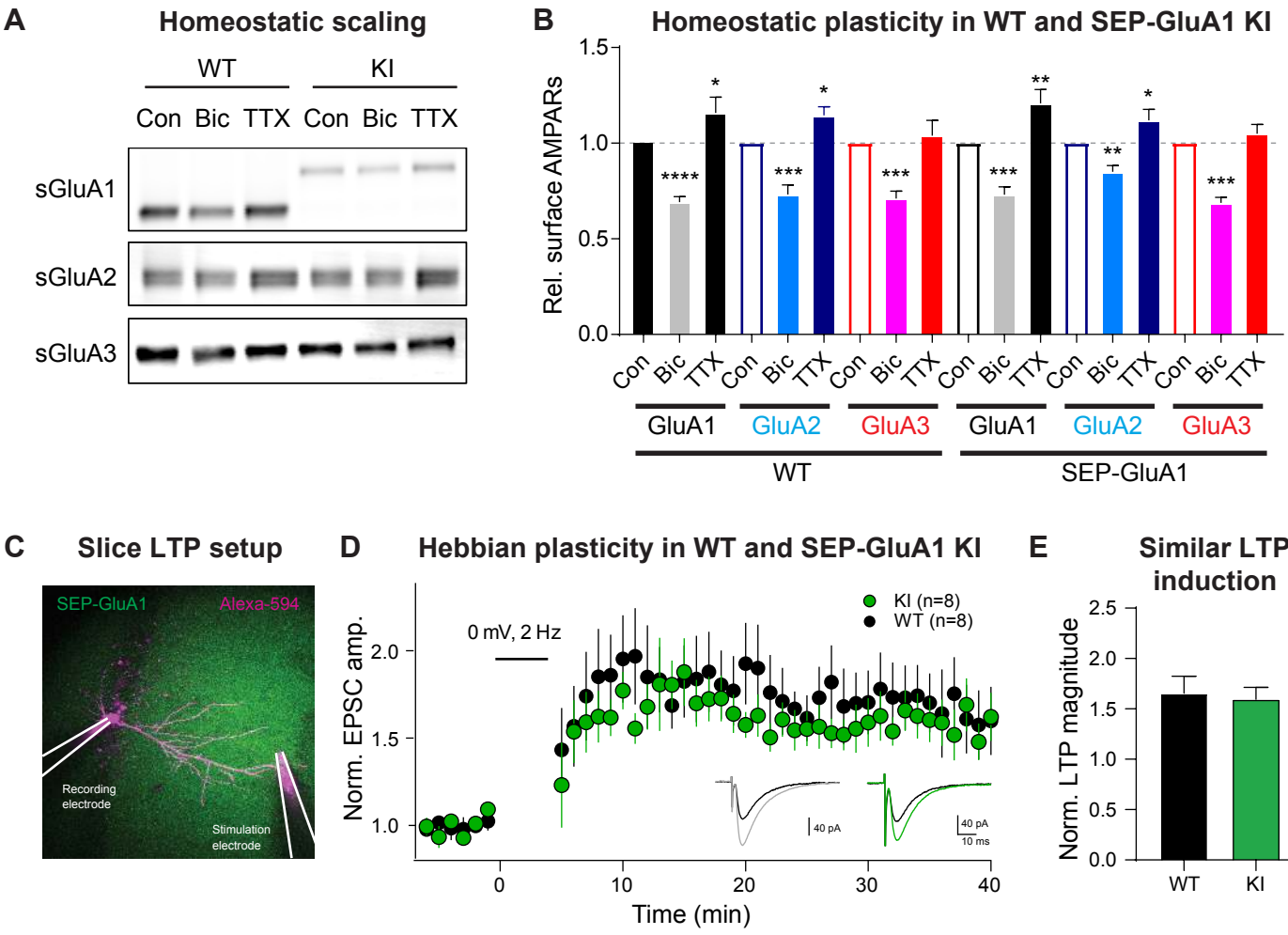


Fig. 3

bioRxiv preprint doi: https://doi.org/10.1101/2020.03.01.972216; this version posted March 2, 2020. The copyright holder for this preprint (which was not certified by peer review) is the author/funder. All rights reserved. No reuse allowed without permission.

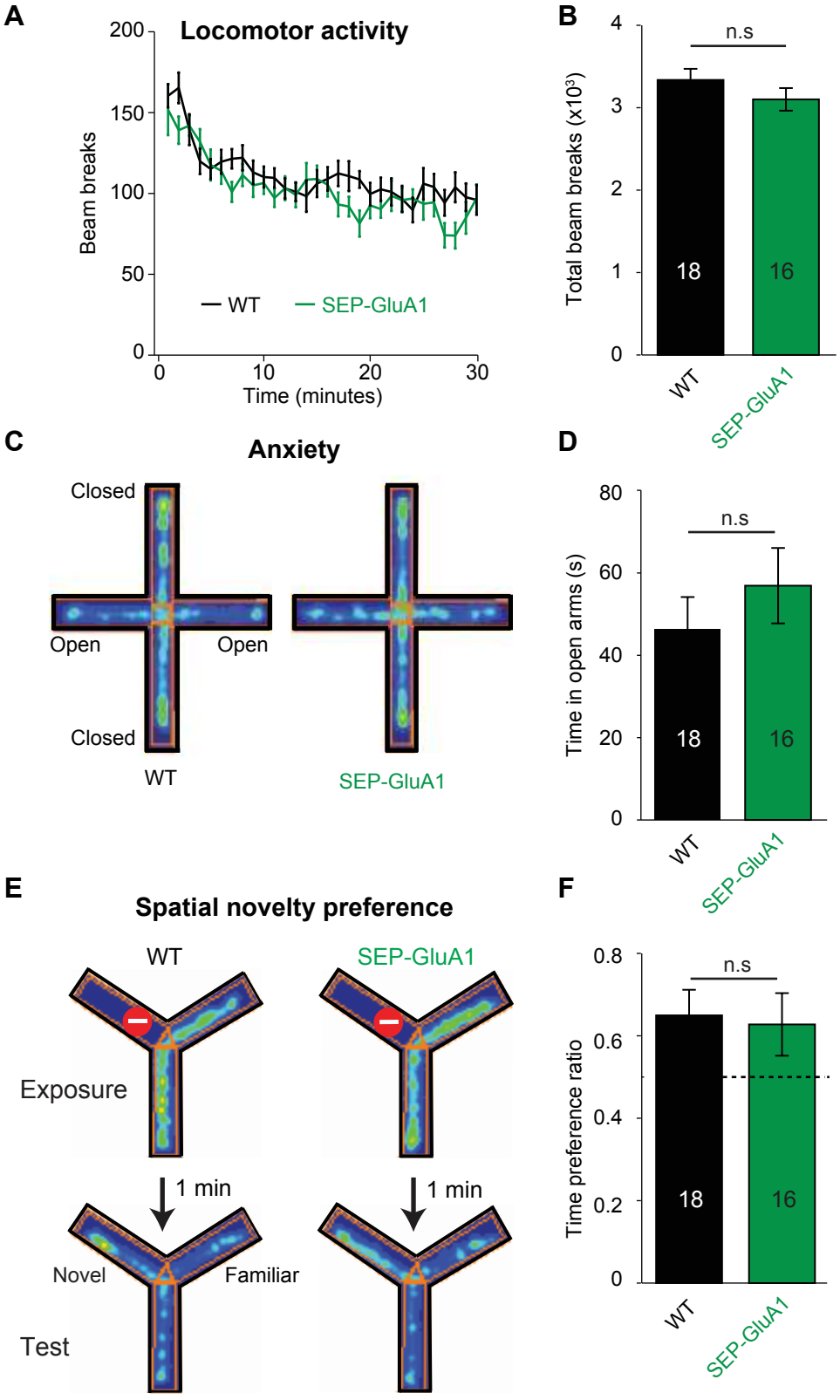


Fig. 4

bioRxiv preprint doi: https://doi.org/10.1101/2020.03.01.972216; this version posted March 2, 2020. The copyright holder for this preprint (which was not certified by peer review) is the author/funder. All rights reserved. No reuse allowed without permission.

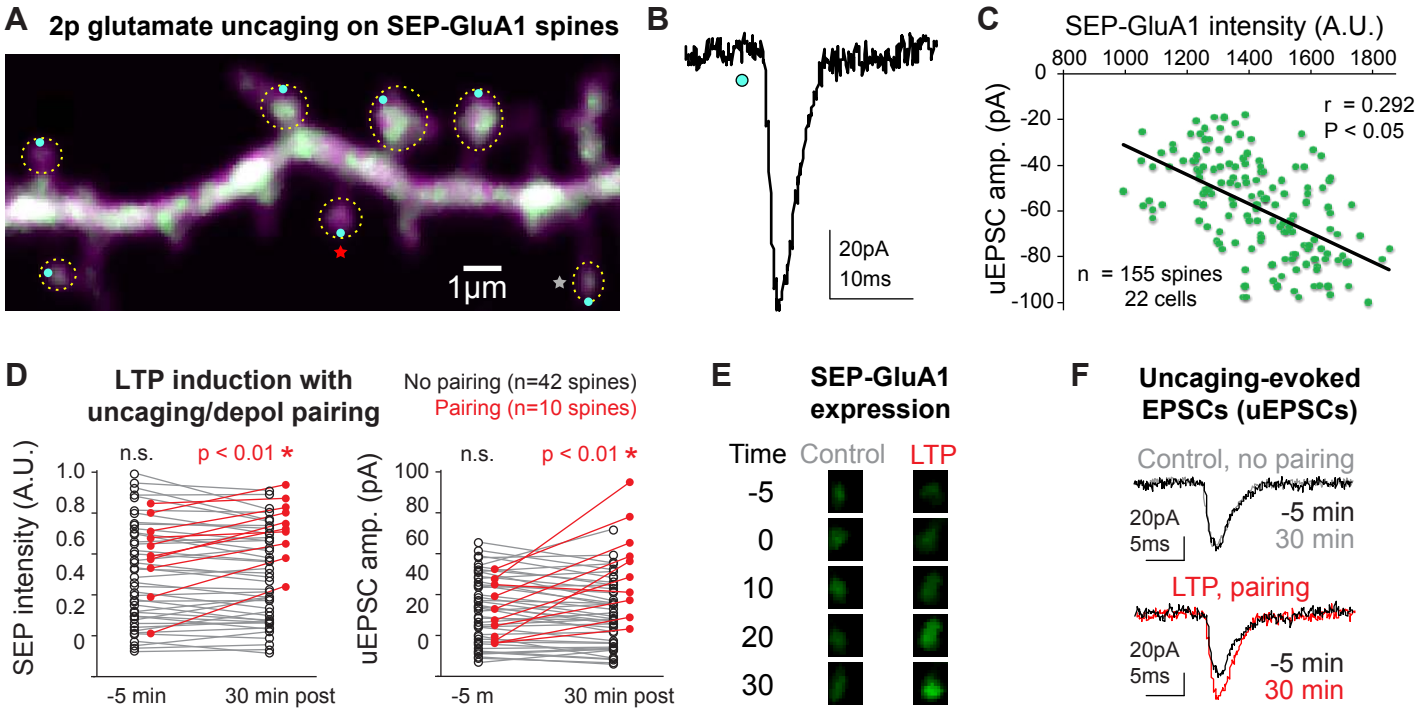


Fig. 5

bioRxiv preprint doi: https://doi.org/10.1101/2020.03.01.972216; this version posted March 2, 2020. The copyright holder for this preprint (which was not certified by peer review) is the author/funder. All rights reserved. No reuse allowed without permission.

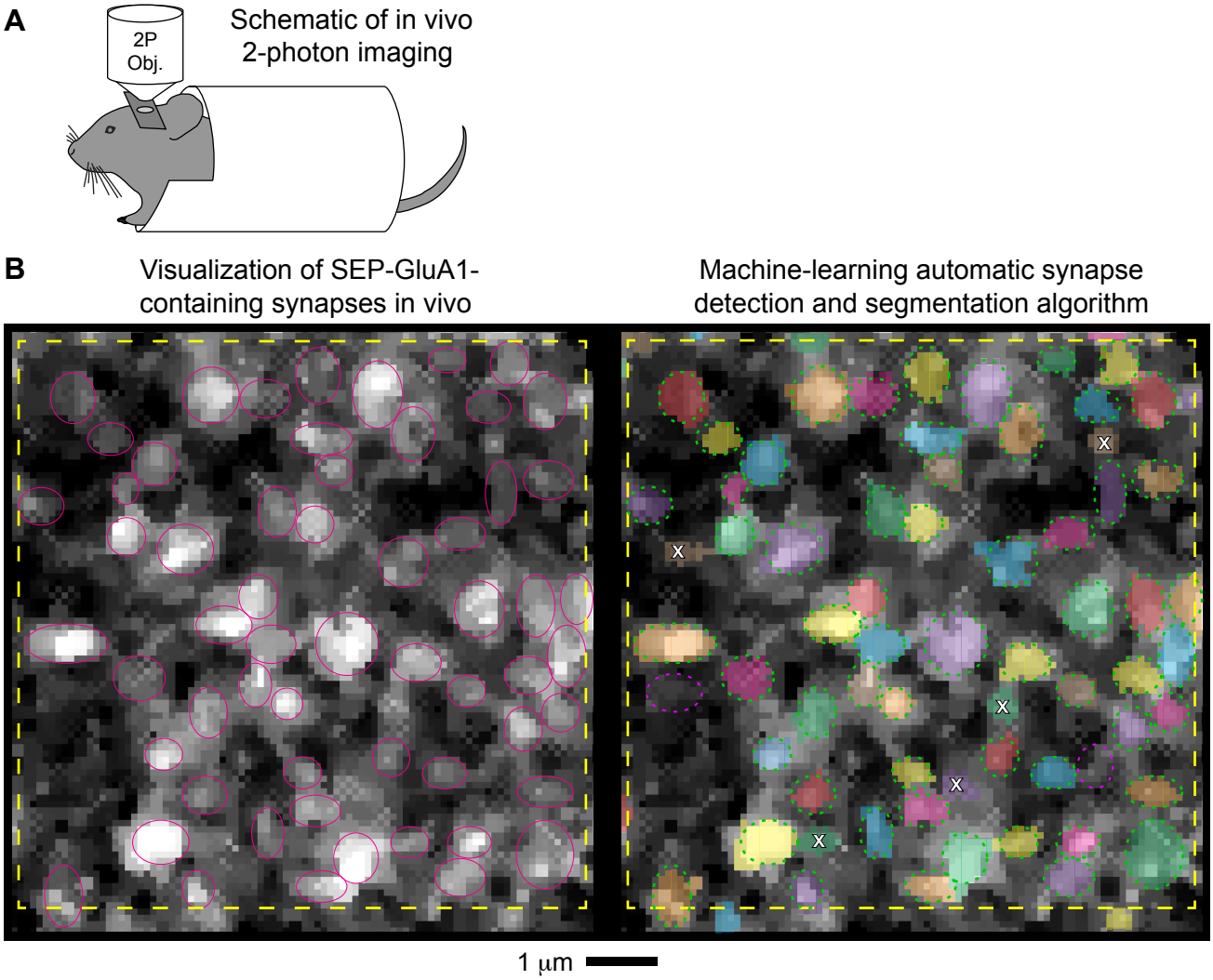


Fig. 6

bioRxiv preprint doi: https://doi.org/10.1101/2020.03.01.972216; this version posted March 2, 2020. The copyright holder for this preprint (which was not certified by peer review) is the author/funder. All rights reserved. No reuse allowed without permission.

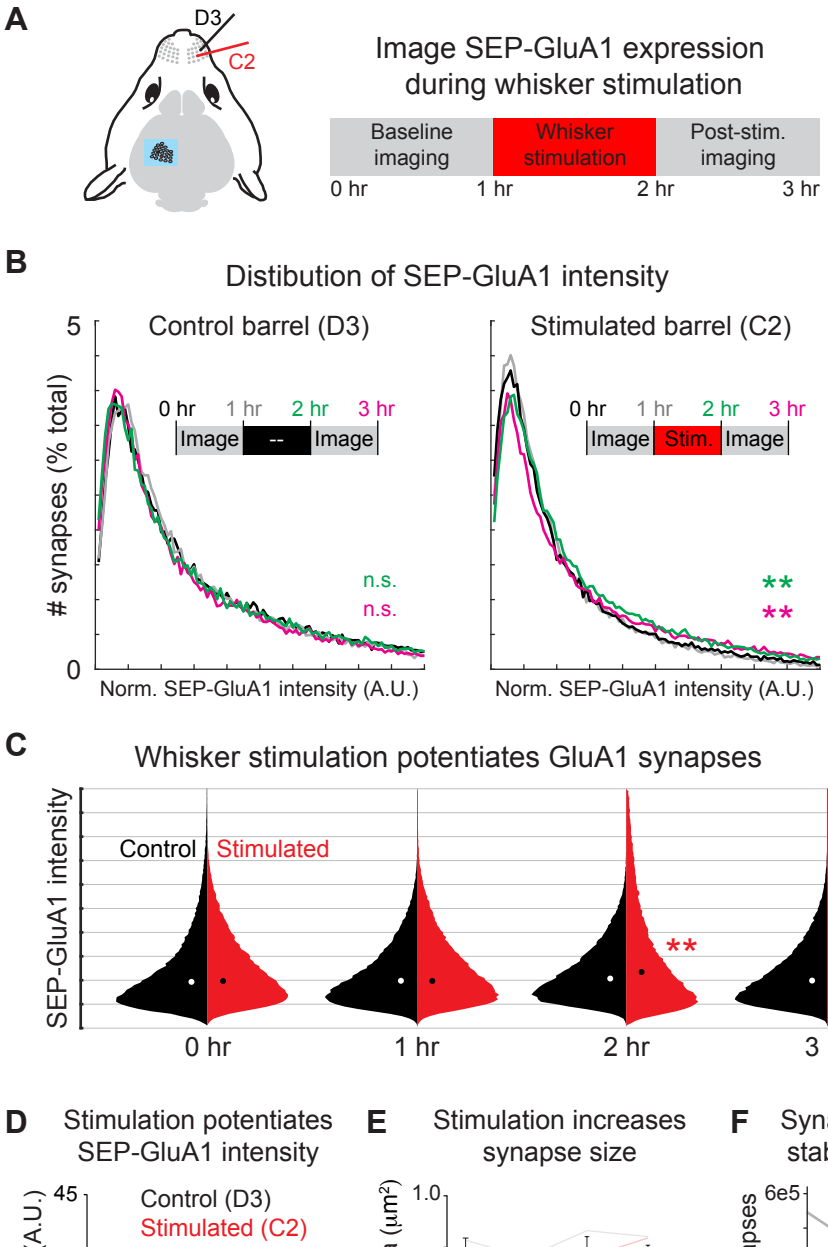


Fig. 7